DIGITAL ACCESS TO
SCHOLARSHIP AT HARVARD
DASH.HARVARD.EDU

HARVARD LIBRARY
Office for Scholarly Communication

Short-Term Hα Variability in M Dwarfs

The Harvard community has made this article openly available. **Please share** how this access benefits you. Your story matters

Short-Term Hα Variability in M Dwarfs

Khee-Gan Lee [1], Edo Berger [2], and Gillian R. Knapp [1]

ABSTRACT

We spectroscopically study the variability of Hα emission in mid- to late-M dwarfs on timescales of $\sim 0.1 - 1$ hr as a proxy for magnetic variability. About 80% of our sample exhibits statistically significant variability on the full range of timescales probed by the observations, and with amplitude ratios in the range of $\sim 1.2 - 4$. No events with an order of magnitude increase in Hα luminosity were detected, indicating that their rate is $\lesssim 0.05$ hr^{-1} (95% confidence level). We find a clear increase in variability with later spectral type, despite an overall decrease in Hα "activity" (i.e., $L_{\mathrm{H}\alpha}/L_{\mathrm{bol}}$). For the ensemble of Hα variability events, we find a nearly order of magnitude increase in the number of events from timescales of about 10 to 30 min, followed by a roughly uniform distribution at longer durations. The event amplitudes follow an exponential distribution with a characteristic scale of Max(EW)/Min(EW) $- 1 \approx 0.7$. This distribution predicts a low rate of $\sim 10^{-6}$ hr^{-1} for events with Max(EW)/Min(EW) $\gtrsim 10$, but serendipitous detections of such events in the past suggests that they represent a different distribution. Finally, we find a possible decline in the amplitude of events with durations of $\gtrsim 0.5$ hr, which may point to a typical energy release in Hα events for each spectral type ($E_{\mathrm{H}\alpha} \sim L_{\mathrm{H}\alpha} \times t \sim$ const). Longer observations of individual active objects are required to further investigate this possibility. Similarly, a larger sample may shed light on whether Hα variability correlates with properties such as age or rotation velocity.

Subject headings: stars: magnetic fields — stars: flare — stars: late-type — stars: activity

---

[1]Department of Astrophysical Sciences, Princeton University, Peyton Hall, Ivy Lane, Princeton, NJ 08544 USA; lee@astro.princeton.edu

[2]Harvard-Smithsonian Center for Astrophysics, 60 Garden Street, Cambridge, MA 02138, USA; eberger@cfa.harvard.edu

1.   Introduction

One of the primary indicators of magnetic heating and activity in low mass stars is Hα chromospheric emission, which traces the presence of gas at temperatures of $\sim 5000 - 10,000$ K. In M dwarfs and later spectral types Hα is a particularly prominent indicator since it is more easily accessible than other chromospheric lines such as Ca II and Mg II, which are located in the faint blue part of the spectrum (e.g., Hawley et al. 1996). Moreover, information on the Hα line is readily available as a by-product of any spectroscopic observations that are used to classify M dwarf properties, such as the TiO band-head at 7050 $\mathring{A}$. Thus, large samples of M dwarfs now exist with measurements of Hα luminosity and its ratio relative to the bolometric luminosity, $L_{H\alpha}/L_{bol}$ (commonly referred to as the Hα "activity").

These samples have led to several important results concerning chromospheric activity in low mass stars. First, the fraction of objects that exhibit Hα in emission increases rapidly from $\sim 5\%$ in the K5–M3 dwarfs to a peak of $\sim 70\%$ around spectral type M7, followed by a subsequent decline in the L dwarfs (Gizis et al. 2000; West et al. 2004, 2008). Second, while the level of activity increases with both rotation and youth in F–K stars, it reaches a saturated value of $L_{H\alpha}/L_{bol} \approx 10^{-3.8}$ in M0–M6 dwarfs, followed by a rapid decline to $L_{H\alpha}/L_{bol} \approx 10^{-5}$ by spectral type L0 (Hawley et al. 1996; Gizis et al. 2000; West et al. 2004). Third, a rotation-activity relation is observed in spectral types earlier than $\sim$ M7, such that essentially all objects with $v \sin(i) \gtrsim 5$ km s^{-1} exhibit saturated Hα activity. However, late-M and L dwarfs exhibit reduced activity even at high rotation rates, $v \sin(i) \gtrsim 10$ km s^{-1} (Mohanty & Basri 2003; Reiners & Basri 2008). Finally, a small fraction ($\lesssim 5\%$) of late-M and L dwarfs have been serendipitously observed to exhibit Hα flares that reach the saturated emission levels found in the earlier-M dwarfs (Liebert et al. 2003).

In this paper we focus on the last point (Hα variability) in the spectral type range M3.5–M8.5, which encompasses the peak of the Hα active fraction, the regime of saturated emission, and the breakdown of the rotation-activity relation. In this spectral type range stars are also fully convective, indicating that the solar-type $\alpha\Omega$ dynamo (e.g., Parker 1955) no longer operates. Thus, studies of Hα temporal variability provide additional constraints on the magnetic dynamo mechanism. While a large number of objects in the mid- and late-M spectral type range have been included in the studies outlined above (for example, $\sim 10^4$ objects in West et al. 2008), Hα variability was not a key aspect of the observations and thus most of the flare and variability detections have been serendipitous in nature. As a result, no systematic results on Hα variability timescales and amplitudes are available in the literature from controlled and uniform cadence observations of a large sample of mid- and late-M dwarfs. Indeed, the few existing studies have only targeted Hα variability in small samples of early M dwarfs. For example, Bopp & Schmitz (1978) studied 15 objects with

spectral types earlier than M4.5 and with a cadence of $\gtrsim 1$ day, while Pettersen et al. (1984) studied Hα variability in only three M3-M3.5 dwarfs. Gizis et al. (2002) studied a larger sample of mid- and late-M dwarfs, but did not use a uniform cadence (or discuss what their cadence was). Finally, observations of a small number of late-M and early-L dwarfs with durations of $\sim 8 - 10$ hr have revealed periodic Hα emission in two objects, tied to their rotation period (Berger et al. 2008, 2009).

Here we present spectroscopic observations of over 40 M3.5–M8.5 dwarfs designed to probe chromospheric variability on timescales of about 5 min to 1 hr. Focusing on the objects that exhibit Hα emission, we find that nearly 80% are variable over the full range of timescales probed by our observations. The outline of the paper is as follows. In §2 we describe the observations and measurements of the Hα equivalent widths and fluxes. We study the Hα emission and its variability in §3, and finally discuss the observed trends and their implications in §4.

2. Observations and Data Reduction

We targeted 43 well-studied M dwarfs in the spectral range M3.5 to M8.5, selected from the samples of Delfosse et al. (1998), Gizis (2002), Mohanty & Basri (2003), Phan-Bao & Bessell (2006), Mohanty & Basri (2003), Cruz et al. (2003), and Crifo et al. (2005). Given the observational setup (see below), we selected targets at a distance of $\lesssim 25$ pc and with an observed magnitude of $V \lesssim 20$ mag. The properties of our selected targets, including luminosities and rotation velocities when available, are summarized in Table 1. Robust ages are not available for our objects, but the small nearby volume of the sample indicates that few objects are expected to be very young. The majority of the objects in our sample have been previously shown to have Hα emission, although only VB 10 was known to exhibit flaring in the chromospheric emission lines.

The observations were carried out using the Boller & Chivens Spectrograph mounted on the du Pont 2.5-m telescope at Las Campanas Observatory, Chile, on two separate occasions: 2007 March 14–17 and 2007 September 12–17. In all observations we used a slit width of $1.5''$, matched to the average seeing conditions, and a 600 lines mm^{-1} grating blazed at 5000 Å . The spectral coverage extended from about 3680 to 6850 Å , designed to cover a wide range of the hydrogen Balmer lines, the Ca II H&K doublet, and the He I lines. The spectral resolution was about 5 Å .

The March 2007 observations were carried out in good weather conditions, with typical seeing of about $1.2''$, while the conditions during the September 2007 observations were

poorer, with strong winds and a typical seeing of about $1.5''$. We observed a total of 20 and 23 objects in the two runs, respectively, with individual exposures of 300 or 600 s (depending on the brightness of the object) and a total observing time of about 1 hr per source. Six of our objects were observed more than once. In total, we obtained over 600 individual spectra spanning ~ 3000 min of total exposure time. A log of the observations is provided in Table 1. The data were reduced using standard routines in `IRAF`, and the wavelength calibration was performed using He-Ar arc lamp exposures.

To measure the Hα equivalent width (EW) in a uniform manner we fit a second-order polynomial to the pseudo-continuum from 6540 to 6620 $\mathring{A}$ (excluding ± 10 $\mathring{A}$ around the Hα emission line). The equivalent widths were then determined by summing the area under the Hα line. The error on each equivalent width measurement includes the noise in the spectrum over the same spectral range, as well as the uncertainty in the continuum fit (using a χ^2 statistic).

3. Hα Equivalent Width Light Curves and Overall Variability

The Hα equivalent width light curves for all individual observations are shown in Figures 1 and 2. We highlight several individual sources in Figure 3. In Table 2 we provide for each source a summary of the median, minimum, maximum, and root-mean-square (RMS) scatter of the Hα equivalent width (EW).

We determine whether a source is variable using a χ^2 test. Namely, we fit a straight line at constant EW through the light curve and calculate the χ^2 value for the best fit. Nine of the objects have light curves that are consistent with non-varying Hα emission on timescales of $\sim 5 - 60$ min at a confidence level greater than 95% (one of them, 2M2226$-$7503, has two separate observations consistent with non-varying emission). These objects are denoted with a '(C)' in the column of RMS values in Table 2; Figure 3a shows the light curve of one such object. We thus conclude that only $\sim 20\%$ of mid- to late-M dwarfs with Hα emission are non-variable on a timescale of $\lesssim 1$ hr.

The rest of the sources ($\sim 80\%$) exhibit a wide range of variability timescales and amplitudes, from rapid variations at the minimum time resolution of our observations (e.g., the M5.5 object 2M0253$-$7959, Figure 3b) to slower variations that span the entire observation (e.g., the M7 object 2M1309$-$2330, Figure 3c). Similarly, the variability amplitudes range from about 1 $\mathring{A}$ to over 20 $\mathring{A}$. Naturally, the sensitivity to small amplitude variations is a function of the signal-to-noise ratio, which in turn depends on the brightness and hence spectral type. The typical variability amplitudes corresponds to fluctuations of about a factor of

two in the Hα luminosity.

We use several indicators to quantify the variability strength. The simplest quantity is $\Delta(\mathrm{EW}) \equiv \mathrm{Max}(\mathrm{EW}) - \mathrm{Min}(\mathrm{EW})$, the difference between the maximum and minimum EW values observed for each object during the course of our observations. However, since the conversion between equivalent width and luminosity depends on the pseudo-continuum brightness (and hence spectral type), this quantity cannot be easily compared across spectral types. To account for the variation in continuum luminosity between spectral types, we use the ratio of the maximum and minimum EW values, $R(\mathrm{EW}) \equiv \mathrm{Max}(\mathrm{EW})/\mathrm{Min}(\mathrm{EW})$, and the RMS normalized by the median equivalent width, $\mathrm{RMS}(\mathrm{EW})/\langle \mathrm{EW} \rangle$. These quantities are plotted as a function of spectral type in Figure 4. In all three cases we find a clear rising trend in variability as a function of spectral type, with an apparent flattening beyond spectral type M7.

The non-varying objects are included in these and subsequent plots for completeness. However, we note that while they may appear to exhibit significant variability as measured by these metrics, their error bars are correspondingly larger. In addition, for several objects we have more than one observation (Table 1). We treat the data for these objects as separate observations in order to maintain a uniform cadence across our sample, although in Table 2 we use the combined data.

The distribution of $\mathrm{RMS}(\mathrm{EW})/\langle \mathrm{EW} \rangle$ as a function of $\langle \mathrm{EW} \rangle$ is shown in Figure 5. We find no clear correlation between the variability and mean equivalent width. The typical value of $\mathrm{RMS}(\mathrm{EW})/\langle \mathrm{EW} \rangle$ is ≈ 0.25, and only about 10% of the objects exceed $\mathrm{RMS}(\mathrm{EW})/\langle \mathrm{EW} \rangle \approx 0.5$.

Finally, we investigate the variability in terms of Hα luminosity. The conversion between EW and $\log(L_{\mathrm{H}\alpha}/L_{\mathrm{bol}})$ is a function of the spectral type since the continuum luminosity declines with later spectral types. Here we adopt the conversion values (so-called χ factor values) from Walkowicz et al. (2004). The resulting mean and maximum values of $\log(L_{\mathrm{H}\alpha}/L_{\mathrm{bol}})$ are listed in Table 2. In Figure 6 we plot the range of maximum and minimum $\log(L_{\mathrm{H}\alpha}/L_{\mathrm{bol}})$ values for each object as a function of spectral type. We recover the same overall declining trend in the mean Hα activity as a function of spectral type demonstrated previously (Hawley et al. 2000; Cruz & Reid 2002; Liebert et al. 2003; West et al. 2004). More interestingly, we clearly find that the level of variability increases with later spectral type, or equivalently with decreasing $\log(L_{\mathrm{H}\alpha}/L_{\mathrm{bol}})$. This result is similarly evident from a comparison of the ratio of maximum to minimum Hα luminosity to the mean Hα luminosity (Figure 7).

4. Individual Variability Events and Timescales

To study the distribution of variability amplitudes and timescales in greater detail, we identify all of the individual variability "events" from the light curves; we do not include the non-variable light curves in this analysis. Events are defined as EW peaks that rise by at least 3σ above the nearest troughs. For example, in Figure 3e, we identify three events — a broad event that lasts from about 10 to 70 min, and two events that last $\lesssim 10$ min at 20 and 35 min. Similarly, we find four events in Figure 3b — a decline in the first 15 min, followed by two short spikes, and finally a gradual rise between 40 and 65 min. The timescale of each event is defined as the time for the Hα EW to transition from a trough through a statistically significant peak to the next trough. In the case of partial events we use the observed timescale and amplitudes as lower limits. We find 71 full events and 27 partial events in the light curves shown in Figures 1 and 2.

A histogram of the variability event timescales is shown in Figure 8a. From the raw event list we find a peak at about 30 min, while partial events are naturally clustered at shorter timescales. The relatively small number of events with durations of ~ 10 min reflects a real trend since such events can be easily detected in our light curves. On the other hand, the decline beyond 30 min, corresponding to timescales longer than about one half of an observing sequence, may reflect the diminishing probability of capturing full events with a duration similar to that of the observation. For example, for our typical observations (1 hr duration with a time resolution of 5 min) the probability of detecting a full 40 min event is only 5/9 of the probability of detecting a full 20 min event. To take this effect into account we normalize each full event bin by its relative probability (Figure 8b).

In addition, to account for the distribution of partial events we make the simple assumption that these events have a uniform probability across all bins with a duration equal to or greater than their measured duration. This assumption is somewhat simplistic given the observed non-uniform trend in the full events, and it is thus likely to under-estimate the true number of events in the $30 - 50$ min bins. However, given the overall number of events this is unlikely to change our conclusions in a significant way

We show the histogram corrected for event detection probability and taking into account the partial events in Figure 8b. As expected, the trend of increased frequency of events between timescales of 10 to 30 min becomes significantly more pronounced, with a factor of 6 times as many events with 30 min duration compared to 10 min duration. The decline at longer timescales is shallower compared to the raw data, with a decline of about 30% relative to the 30 min bin (compared to $60 - 90\%$ in the raw distribution). Taking into account our simple prescription of assigning partial events, it is likely that the distribution is in fact flat on timescales of $30 - 60$ min.

We next turn to the event amplitude ratios. We focus on this quantity since it can be uniformly compared across spectral types. We plot the histogram of R(EW) values in Figure 9. The distribution exhibits an exponential decline in the number of events (N) as a function of amplitude ratio, with

$$N \propto \exp\left(-\frac{R(\text{EW}) - 1}{0.7}\right). \tag{1}$$

We note that this fit does not include partial events. To investigate whether there is a difference in the distribution as a function of spectral type, we divide the sample into two subsets split at M6 and repeat the analysis of timescale and amplitude distributions. We find the two sub-samples to be indistinguishable, indicating that there no obvious trend in Hα variability amplitude and timescale for individual events.

Finally, we search for a correlation between the event durations and amplitudes. Figure 10 shows the event amplitude ratios plotted against their durations. We find that R(EW) generally increases with increased timescale, but this effect is only apparent on timescales shorter than about 30 min. Longer events tend to have lower amplitudes. However, partial events are likely to increase the number of long duration, high amplitude events, potentially leading to a flatter distribution beyond 30 min.

5. Discussion and Conclusions

We carried out spectroscopic observations of 43 M dwarfs in the range M3.5–M8.5, for approximately 1 hour each with a time resolutions of about 5 min. About 80% of our targets exhibit statistically significant Hα variability, ranging from a factor of 1.25 to about 4. Based on a total on-source exposure time of about 3000 min we find that the duty cycle of flares with an order of magnitude increase in brightness is $\lesssim 0.05$ hr^{-1} (95% confidence level, assuming Poisson distribution). This limit is similar to previous results for individual well-studied objects (e.g., LHS2065; Martín & Ardila 2001).

The level of variability for individual objects is found to increase with later spectral type, with a possible flattening beyond $\sim$ M7. In terms of Hα luminosity, we recover the familiar trend of decreasing $L_{\text{H}\alpha}/L_{\text{bol}}$ with later spectral type. More importantly, however, we find that the range of light curve variability increases with later spectral type, such that M7–M8 objects exhibit a range of about 0.5 dex in $L_{\text{H}\alpha}/L_{\text{bol}}$ compared to only 0.15 dex for M4–M5 objects. This result indicates that while the traditional definition of "activity" (i.e., $L_{\text{H}\alpha}/L_{\text{bol}}$) declines with later spectral type, the actual fluctuations in activity increase with later spectral type.

The individual light curves exhibit a rich phenomenology, with activity timescales spanning the full range covered by our observations, i.e., $\sim 5 - 60$ min. We find that fluctuations on timescales of ~ 10 min are significantly less common than those on ~ 30 min timescale, and that longer duration events (at least to ~ 1 hr) are likely to be as common. The event amplitude ratios closely follow an exponential distribution with a characteristic value of $R(\mathrm{EW}) - 1 \approx 0.7$. Taken at face value, this means that events with an amplitude ratio of 10 are $\sim 10^5$ times less common than those with a ratio of 2. Thus, our observed rate of about 0.1 event per hour with a factor of 2 increase in EW implies an expected rate of $\sim 10^{-6}$ hr^{-1} for events with an order of magnitude increase in EW. The fact that several such events are published in the literature (e.g., Martín & Ardila 2001) suggests that major flare events are not drawn from the same statistical distribution of mild variability events found in our work. Indeed, Schmidt et al. (2007) estimate that events with $\Delta(\mathrm{EW}) \gtrsim 15$ Å have a duty cycle of $\sim 5\%$ in late-M dwarfs, orders of magnitude larger than expected from our exponential distribution (however, $\Delta(\mathrm{EW})$ depends on spectra type so a direct comparison is challenging).

Combining the event amplitudes and timescales, we do not find any clear correlations, although there appears to be a general trend of declining amplitude for longer duration events. Such a relation would be expected if Hα events in each spectral type released similar amounts of total magnetic energy such that $E_{\mathrm{H}\alpha} \sim L_{\mathrm{H}\alpha} \times t \propto \mathrm{EW} \times t \sim$ const. On the other hand, the opposite trend would be expected if Hα events represent the release of magnetic stresses in the chromosphere such that frequent and/or shorter duration events will have lower amplitude. It remains to be seen from observations with longer time baselines which effect exists, and whether it correlates with spectral type.

The large and growing samples of nearby M dwarfs are conducive for a continued systematic investigation of Hα emission as a proxy for magnetic activity. Clearly, Hα variability at the level of $\lesssim 2$ is prevalent in the bulk of Hα-emitting mid- and late-M dwarfs on timescales of $\sim 0.1 - 1$ hr. Future observations will need to address three primary questions:

1. Are the durations and amplitudes of Hα events correlated? If so, directly or inversely?

2. Are large flares drawn from the same distribution as small events?

3. Are the prevalence and properties of events/flares correlated with age or rotation velocity across the M spectral type range?

To address these questions we will continue to pursue observations of larger samples, as well as longer time baseline observations of individual active objects.

REFERENCES

Berger, E., et al. 2008, ApJ, 673, 1080

Berger, E., et al. 2009, ApJ, 695, 310

Bochanski, J. J., Hawley, S. L., Reid, I. N., Covey, K. R., West, A. A., Tinney, C. G., & Gizis, J. E. 2005, AJ, 130, 1871

Bopp, B. W., & Schmitz, M. 1978, PASP, 90, 531

Crifo, F., Phan-Bao, N., Delfosse, X., Forveille, T., Guibert, J., Martín, E. L., & Reylé, C. 2005, A&A, 441, 653

Cruz, K. L., & Reid, I. N. 2002, AJ, 123, 2828

Cruz, K. L., Reid, I. N., Liebert, J., Kirkpatrick, J. D., & Lowrance, P. J. 2003, AJ, 126, 2421

Delfosse, X., Forveille, T., Perrier, C., & Mayor, M. 1998, A&A, 331, 581

Gizis, J. E., Monet, D. G., Reid, I. N., Kirkpatrick, J. D., Liebert, J., & Williams, R. J. 2000, AJ, 120, 1085

Gizis, J. E. 2002, ApJ, 575, 484

Gizis, J. E., Reid, I. N., & Hawley, S. L. 2002, AJ, 123, 3356

Hawley, S. L., Gizis, J. E., & Reid, I. N. 1996, AJ, 112, 2799

Hawley, S., Reid, I. N., & Gizis, J. 2000, From Giant Planets to Cool Stars, 212, 252

Henry, T. J. and Kirkpatrick, J. D. & Simons, D. A. 1994, AJ, 108, 1437

Herbig, G. H. 1956, PASP, 68, 531

Liebert, J., Kirkpatrick, J. D., Cruz, K. L., Reid, I. N., Burgasser, A., Tinney, C. G., & Gizis, J. E. 2003, AJ, 125, 343

Liebert, J., Kirkpatrick, J. D., Reid, I. N., & Fisher, M. D. 1999, ApJ, 519, 345

Lodieu, N., Scholz, R.-D., McCaughrean, M. J., Ibata, R., Irwin, M., & Zinnecker, H. 2005, A&A, 440, 1061

Martín, E. L., & Ardila, D. R. 2001, AJ, 121, 2758

Mohanty, S., & Basri, G. 2003, ApJ, 583, 451

Parker, E. N. 1955, ApJ, 122, 293

Pettersen, B. R., Coleman, L. A., & Evans, D. S. 1984, ApJ, 282, 214

Phan-Bao, N., & Bessell, M. S. 2006, A&A, 446, 515

Reid, I. N., Kirkpatrick, J. D., Liebert, J., Gizis, J. E., Dahn, C. C., & Monet, D. G. 2002, AJ, 124, 519

Reid, I. N., et al. 2003, AJ, 126, 3007

Reid, I. N., et al. 2004, AJ, 128, 463

Reid, I. N., & Gizis, J. E. 2005, PASP, 117, 676

Reiners, A. & Basri, G. 2008, ArXiv e-prints, 805

Schmidt, S. J., Cruz, K. L., Bongiorno, B. J., Liebert, J., & Reid, I. N. 2007, AJ, 133, 2258

Scholz, R.-D., Lo Curto, G., Méndez, R. A., Hambaryan, V., Costa, E., Henry, T. J., & Schwope, A. D. 2005, A&A, 439, 1127

Scholz, R.-D., Meusinger, H., & Jahreiß, H. 2005, A&A, 442, 211

Walkowicz, L. M., Hawley, S. L., & West, A. A. 2004, PASP, 116, 1105

West, A. A., et al. 2004, AJ, 128, 426

West, A. A., Hawley, S. L., Bochanski, J. J., Covey, K. R., Reid, I. N., Dhital, S., Hilton, E. J., & Masuda, M. 2008, AJ, 135, 785

Wilking, B. A., Greene, T. P., & Meyer, M. R. 1999, AJ, 117, 469

Table 1.   Source Properties and Log of Observations

Source	Other	Sp. Type	Date [a] (UT)	Exposures (s)	$\log(L_{\rm bol}/L_\odot)$ [b]	d (pc)	$v \sin i$ (km s^{-1})	Ref. [c]
G 99-049	GJ 3379	M3.5	Mar 15 23:58:23	12×300	-1.63	5.4	7.4	1, *8*
LHS 1723	⋯	M4	Mar 14 00:01:34	11×300	-1.92	6.1	<3.2	2, *8*
L 449-1	⋯	M4	Mar 14 01:00:14	11×300	⋯	5.7	⋯	3
GJ 1224	⋯	M4.5	Mar 14 08:29:12	14×300	-2.36	7.5	<5.6	2, *8*
GL 285	V* YZ CMi	M4.5	Mar 15 01:10:51	13×300	-1.52	6.2	6.5	2, *8*
2MASSW J1013426-275958	⋯	M5	Mar 14 04:28:58	6×600	⋯	⋯	⋯	4, *8*
GJ 1156	V* GL Vir	M5	Mar 14 05:57:50	12×300	-2.30	6.5	9.2	2, *8*
GJ 1154A	⋯	M5	Mar 15 03:41:37	18×300	⋯	8.5	5.2	2, *8*
DENIS-P J213422.2-431610	⋯	M5.5	Sep 12 04:12:02	4×300	⋯	14.6	⋯	5
2MASS J02591181+0046468	⋯	M5.5	Sep 14 04:48:39	11×300	-3.61	29	⋯	6
2MASS J02534448-7959133	⋯	M5.5	Sep 14 06:21:38	13×300	-3.44	17.2	⋯	7
2MASS J00244419-2708242	GJ 2005	M5.5	Sep 14 07:42:30	12×300	-2.59	7.5	9.0	8, *8*
			Sep 15 03:20:25	10×300				
			Sep 15 06:14:05	38×300				
2MASS J00045753-1709369	⋯	M5.5	Sep 15 00:52:58	9×300	-3.31	14.9	⋯	5
2MASS J20021341-5425558	⋯	M5.5	Sep 12 02:51:06	11×300	-3.55	17.2	⋯	7
LP 844-25	LHS 2067	M6	Mar 14 03:19:25	6×600	-3.90	25.1	⋯	9
2MASS J16142520-0251009	LP 624-54	M6	Mar 17 08:34:42	15×300	-3.42	14.6	⋯	7
			Sep 13 23:47:29	10×300				
2MASS J21322975-0511585	NLTT 51488	M6	Sep 14 23:52:34	6×300	-3.47	18.5	⋯	7
2MASS J23373831-1250277	NLTT 57439	M6	Sep 14 01:47:33	16×300	-3.49	19.2	⋯	10
2MASSW J1012065-304926	⋯	M6	Mar 17 01:13:30	6×600	⋯	⋯	⋯	4
LP 731-47	⋯	M6	Mar 17 04:29:30	12×300	⋯	20.5	11.0	7, *8*
2MASS J23155449-0627462	NLTT 56283	M6	Sep 16 00:40:42	9×300	-3.37	17.7	⋯	11
2MASS J20424514-0500193	NLTT 49734	M6.5	Sep 13 03:32:18	12×300	-3.51	15.5	⋯	12
GJ 3622	⋯	M6.5	Mar 15 05:25:04	12×300	⋯	4.5	3.0	1, *8*
2MASS J05023867-3227500	⋯	M6.5	Mar 16 23:56:31	12×300	-3.89	25.1	⋯	10
2MASS J02141251-0357434	LHS 1363	M6.5	Sep 13 09:01:56	10×300	-3.11	10.1	⋯	10
			Sep 14 03:25:22	4×300				
2MASS J10031918-0105079	LHS 5165	M7	Mar 14 02:08:39	6×600	-3.84	23.1	⋯	10
2MASS J13092185-2330350	⋯	M7	Mar 14 07:11:58	6×600	-3.62	13.3	7.0	4, *13*
2MASSW J1032136-420856	⋯	M7	Mar 15 02:42:22	6×600	⋯	⋯	⋯	4
2MASSW J1420544-361322	⋯	M7	Mar 15 06:37:15	8×300	⋯	⋯	⋯	4
2MASS J09522188-1924319	⋯	M7.5	Mar 16 02:26:22	10×450	-3.68	⋯	6.0	13, *13*
			Mar 17 23:45:15	8×600				
2MASS J04291842-3123568	⋯	M7.5	Sep 12 07:12:29	12×300	-3.26	11.4	⋯	14
2MASS J23062928-0502285	⋯	M7.5	Sep 13 05:11:27	6×600	-3.46	11.0	⋯	10
2MASS J03313025-3042383	NLTT 11163	M7.5	Sep 13 06:28:07	6×600	-3.46	12.1	⋯	10
2MASS J04351612-1606574	NLTT 13580	M7.5	Sep 13 07:44:12	12×300	-3.09	8.6	⋯	15
2MASS J06572547-4019134	⋯	M7.5	Mar 16 01:22:06	6×600	-4.01	22.7	⋯	10
2MASS J05173766-3349027	⋯	M8	Sep 12 08:27:48	9×600	-3.71	14.7	⋯	10
2MASS J19165762+0509021	VB 10	M8	Sep 13 00:54:33	12×300	-2.88	5.7	6.5	8, *8*
2MASS J22062280-2047058	⋯	M8	Sep 14 00:35:30	6×600	-3.88	18.2	22.0	10, *8*
			Sep 15 23:39:08	6×600				
2MASS J02484100-1651216	⋯	M8	Sep 14 09:10:55	4×600	-3.94	16.2	⋯	10

Table 1—Continued

Source	Other	Sp. Type	Date [a] (UT)	Exposures (s)	$\log(L_{\mathrm{bol}}/L_\odot)$ [b]	d (pc)	$v\sin i$ (km s^{-1})	Ref. [c]
2MASS J20370715-1137569	$\cdots$	M8	Sep 16 23:39:45	5×600	-3.85	16.8	$\cdots$	10
2MASS J22264440-7503425	$\cdots$	M8.5	Sep 12 01:26:16	6×600	-3.87	16.5	$\cdots$	5
			Sep 15 04:35:01	6×600				
2MASS J03061159-3647528	$\cdots$	M8.5	Sep 12 04:50:23	5×600	-3.61	11.3	$\cdots$	5
2MASS J23312174-2749500	$\cdots$	M8.5	Sep 13 02:13:20	6×600	-3.61	11.6	$\cdots$	5

[a]All observations were carried out in the year 2007.

[b]Bolometric luminosities were derived using bolometric corrections on the J and K magnitudes listed in the SIMBAD database, using the fits described in Wilking et al. (1999).

[c]References for spectral types are in standard font; references for rotational velocities are in italics: [1] Henry et al. (1994); [2] Delfosse et al. (1998); [3] Scholz et al. (2005a); [4] Gizis (2002); [5] Crifo et al. (2005); [6] Bochanski et al. (2005); [7] Phan-Bao & Bessell (2006); [8] Mohanty & Basri (2003); [9] Reid & Gizis (2005); [10] Cruz et al. (2003); [11] Scholz et al. (2005b); [12] Reid et al. (2004); [13] Reid et al. (2002); [14] Schmidt et al. (2007); [15] Lodieu et al. (2005).

Table 2. Hα Variability

Source	Sp. Type	Published EW	Ref.[a]	⟨EW⟩[b]	Min(EW)	Max(EW)	Δ(EW)[c]	RMS(EW)[d]	Mean $\log(L_{\mathrm{H\alpha}}/L_{\mathrm{bol}})$	Max $\log(L_{\mathrm{H\alpha}}/L_{\mathrm{bol}})$
		(Å)		(Å)	(Å)	(Å)	(Å)	(Å)		
G 99-049	M3.5	2.9	1	7.1 ± 0.1	7.0 ± 0.1	8.1 ± 0.1	1.1 ± 0.1	0.5 ± 0.1	-3.229	-3.178
LHS 1723	M4	0.9	1	1.2 ± 0.2	1.0 ± 0.1	1.3 ± 0.1	0.3 ± 0.2	0.1 ± 0.1(C)	-4.155	-4.082
L 449-1	M4	· · ·	· · ·	6.8 ± 0.2	6.7 ± 0.1	7.1 ± 0.1	0.4 ± 0.2	0.1 ± 0.1(C)	-3.357	-3.345
GJ 1224	M4.5	2.3	1	4.8 ± 0.2	4.3 ± 0.2	5.2 ± 0.2	0.9 ± 0.2	0.2 ± 0.2	-3.480	-3.436
GL 285	M4.5	9.5	1	9.3 ± 0.1	8.6 ± 0.1	10.6± 0.1	2.0 ± 0.1	0.6 ± 0.1	-3.179	-3.152
2MASSW J1013426-275958	M5	6.6	2	7.2 ± 0.4	6.5 ± 0.4	7.8 ± 0.3	1.3 ± 0.5	0.4 ± 0.3(C)	-3.711	-3.670
GJ 1156	M5	4.4	1	6.9 ± 0.3	6.4 ± 0.2	8.8 ± 0.2	2.3 ± 0.3	0.7 ± 0.2	-3.705	-3.618
GJ 1154A	M5	4.3	1	8.9 ± 0.3	6.8 ± 0.2	13.5± 0.2	6.6 ± 0.2	2.0 ± 0.2	-3.589	-3.448
DENIS-P J213422.2-431610	M5.5	· · ·	· · ·	0.9 ± 0.5	0.6 ± 0.3	1.6 ± 0.3	1.1 ± 0.4	0.4 ± 0.4(C)	-4.466	-4.262
2MASS J02591181+0046468	M5.5	14.5	3	12.0 ± 0.8	9.3 ± 0.7	15.2± 0.4	5.8 ± 0.8	1.9 ± 0.6	-3.387	-3.290
2MASS J02534448-7959133	M5.5	12.4	4	7.8 ± 0.3	6.3 ± 0.4	12.2± 0.6	5.9 ± 0.7	1.9 ± 0.5	-3.502	-3.387
2MASS J00244419-2708242	M5.5	3.6	1	4.0 ± 4.5	1.8 ± 4.5	8.5 ± 0.3	6.7 ± 4.5	1.1 ± 0.7	-3.734	-3.537
2MASS J00045753-1709369	M5.5	· · ·	· · ·	4.4 ± 0.4	3.0 ± 0.3	5.9 ± 0.4	2.9 ± 0.5	0.8 ± 0.4	-3.813	-3.695
2MASS J20021341-5425558	M5.5	7.6	4	1.9 ± 0.4	3.5 ± 0.8	7.5 ± 0.5	4.0 ± 0.9	1.3 ± 0.6	-3.785	-3.591
LP 844-25	M6	· · ·	· · ·	6.7 ± 1.2	1.0 ± 0.3	2.3 ± 0.3	1.2 ± 0.4	0.5 ± 0.3	-4.610	-4.394
2MASS J16142520-0251009	M6	4.2	4	8.5 ± 0.9	1.9 ± 0.7	5.9 ± 0.6	3.9 ± 0.9	1.0 ± 0.6	-4.187	-3.985
2MASS J21322975-0511585	M6	1.1	4	3.5 ± 0.8	0.1 ± 0.5	1.4 ± 0.5	1.4 ± 0.7	0.6 ± 0.5	-5.057	-4.610
2MASS J23373831-1250277	M6	· · ·	· · ·	3.1 ± 0.7	14.6± 0.5	25.9± 0.6	11.3± 0.8	4.9 ± 0.5	-3.500	-3.358
2MASSW J1012065-304926	M6	5.6	2	12.5 ± 0.7	4.6 ± 0.7	10.4± 0.4	5.8 ± 0.8	2.2 ± 0.7	-3.904	-3.756
LP 731-47	M6	6.4	4	0.6 ± 0.7	4.8 ± 0.7	11.4± 1.0	6.6 ± 1.2	2.0 ± 0.7	-3.847	-3.714
2MASS J23155449-0627462	M6	1.1	5	5.0 ± 0.4	3.4 ± 0.9	5.9 ± 0.7	2.5 ± 1.2	1.1 ± 0.8	-4.122	-3.985
2MASS J20424514-0500193	M6.5	· · ·	· · ·	4.1 ± 0.4	2.1 ± 0.5	4.5 ± 0.4	2.4 ± 0.6	0.6 ± 0.5	-4.451	-4.341
GJ 3622	M6.5	1.9	1	7.7 ± 0.8	3.4 ± 0.3	4.6 ± 0.3	1.1 ± 0.4	0.3 ± 0.3(C)	-4.393	-4.332
2MASS J05023867-3227500	M6.5	· · ·	· · ·	3.3 ± 0.7	7.4 ± 0.5	12.3± 2.5	4.9 ± 2.5	2.5 ± 1.0	-4.050	-3.915
2MASS J02141251-0357434	M6.5	· · ·	· · ·	7.2 ± 0.4	6.9 ± 0.3	18.3± 0.5	11.5± 0.6	3.7 ± 0.4	-4.012	-3.732
2MASS J10031918-0105079	M7	· · ·	· · ·	10.6 ± 1.2	8.9 ± 0.9	17.4± 0.7	8.4 ± 1.1	2.9 ± 0.8	-4.201	-4.050
2MASS J13092185-2330350	M7	6.7	2	6.0 ± 0.9	5.1 ± 0.6	9.3 ± 0.5	4.2 ± 0.8	1.5 ± 0.6	-4.383	-4.312
2MASSW J1032136-420856	M7	11.8	2	11.9 ± 1.3	11.9± 1.3	19.9± 1.4	8.0 ± 1.9	3.7 ± 1.4	-4.201	-4.002
2MASSW J1420544-361322	M7	7.0	2	16.5 ± 1.2	8.5 ± 0.6	30.0± 0.5	21.6± 0.8	8.5 ± 0.8	-4.050	-3.804
2MASS J09522188-1924319	M7.5	11.3	6	4.5 ± 2.1	8.1 ± 0.6	18.9± 0.3	10.8± 0.7	3.1 ± 0.4	-3.940	-3.736
2MASS J04291842-3123568	M7.5	15.9	7	10.9 ± 0.7	10.8± 0.4	14.8± 0.5	3.9 ± 0.6	1.2 ± 0.5	-3.933	-3.866
2MASS J23062928-0502285	M7.5	2.8	7	12.6 ± 0.5	3.4 ± 0.7	5.4 ± 0.8	2.0 ± 1.1	0.8 ± 0.7(C)	-4.379	-4.280
2MASS J03313025-3042383	M7.5	7.6	7	3.5 ± 0.9	7.4 ± 0.6	10.9± 0.6	3.5 ± 0.8	1.5 ± 0.7	-4.068	-4.012

Table 2—Continued

Source	Sp. Type	Published EW (Å)	Ref.[a]	$\langle$EW$\rangle$[b] (Å)	Min(EW) (Å)	Max(EW) (Å)	Δ(EW)[c] (Å)	RMS(EW)[d] (Å)	Mean $\log(L_{H\alpha}/L_{bol})$	Max $\log(L_{H\alpha}/L_{bol})$
2MASS J04351612-1606574	M7.5	3.7	6	7.8 ± 1.0	5.3 ± 0.8	8.3 ± 0.4	2.9 ± 0.8	0.9 ± 0.6	-4.206	-4.093
2MASS J06572547-4019134	M7.5	$\cdots$	$\cdots$	5.7 ± 0.8	4.4 ± 1.2	11.8± 1.7	7.4 ± 2.1	2.5 ± 1.8	-4.180	-3.971
2MASS J05173766-3349027	M8	8.1	4	2.7 ± 1.6	1.5 ± 1.2	5.4 ± 1.1	3.9 ± 1.6	1.3 ± 1.1(C)	-4.688	-4.487
2MASS J19165762+0509021	M8	5.6	1	4.7 ± 0.8	3.8 ± 0.5	8.8 ± 0.5	5.1 ± 0.7	1.3 ± 0.5	-4.479	-4.275
2MASS J22062280-2047058	M8	5.1	8	3.6 ± 1.3	2.3 ± 0.9	12.5± 1.2	10.2± 1.5	2.9 ± 1.1	-4.356	-4.123
2MASS J02484100-1651216	M8	7.9	7	6.5 ± 1.2	2.1 ± 1.3	7.4 ± 1.0	5.3 ± 1.7	1.9 ± 1.2	-4.538	-4.350
2MASS J20370715-1137569	M8	6.2	7	1.8 ± 1.3	0.7 ± 0.7	2.1 ± 1.4	1.4 ± 1.5	0.5 ± 1.2(C)	-5.016	-4.897
2MASS J22264440-7503425	M8.5	3.2	7	0.6 ± 2.4	3.3 ± 1.1	11.7± 1.5	8.4 ± 1.9	2.7 ± 1.7(C)	-4.538	-4.350
2MASS J03061159-3647528	M8.5	0.5	6	8.3 ± 0.7	3.9 ± 0.8	12.1± 0.7	8.1 ± 1.1	2.6 ± 0.8	-4.421	-4.239
2MASS J23312174-2749500	M8.5	5.1	6	5.5 ± 1.0	3.5 ± 0.9	7.1 ± 0.7	3.6 ± 1.1	1.1 ± 0.9	-4.594	-4.467

[a]References for the published EWs: (1) Mohanty & Basri (2003) (2) Gizis (2002) (3) Bochanski et al. (2005) (4) Phan-Bao & Bessell (2006) (5) Reid et al. (2003) (6) Lodieu et al. (2005) (7) Schmidt et al. (2007) (8) Reid et al. (2002)

[b]Median EW.

[c]Δ(EW) $\equiv$ Max(EW) $-$ Min(EW)

[d]'(C)' denotes that the object's EW was constant within errors during the observations (see discussion in Section 3). Note that while 2M2226-7503 had two separate observations, both lightcurves were found to be consistent with a constant EW.
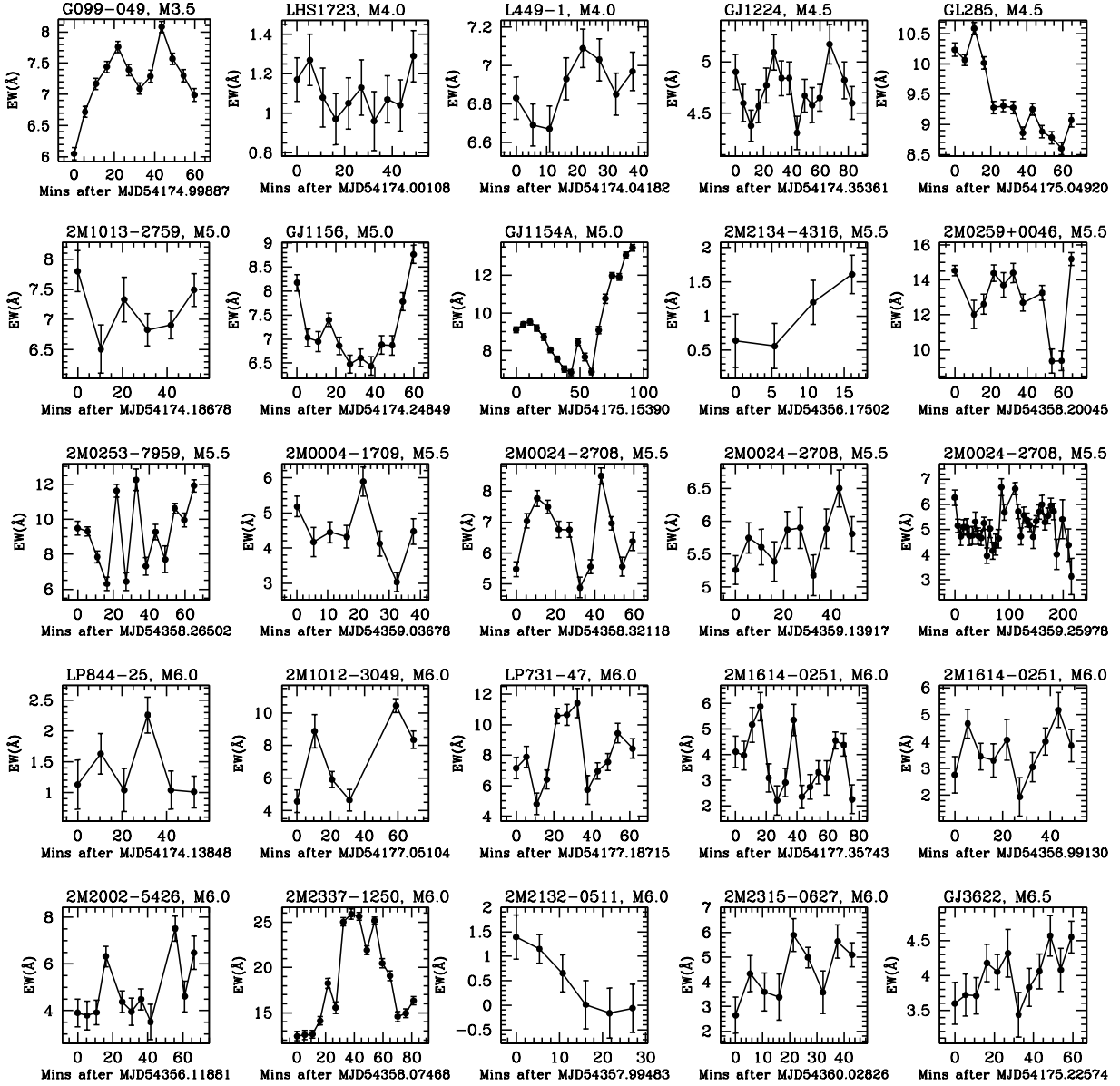
Fig. 1.— Hα EWs plotted against time in minutes, for all observations in our sample. Note that some objects have several light curves from repeated observations.
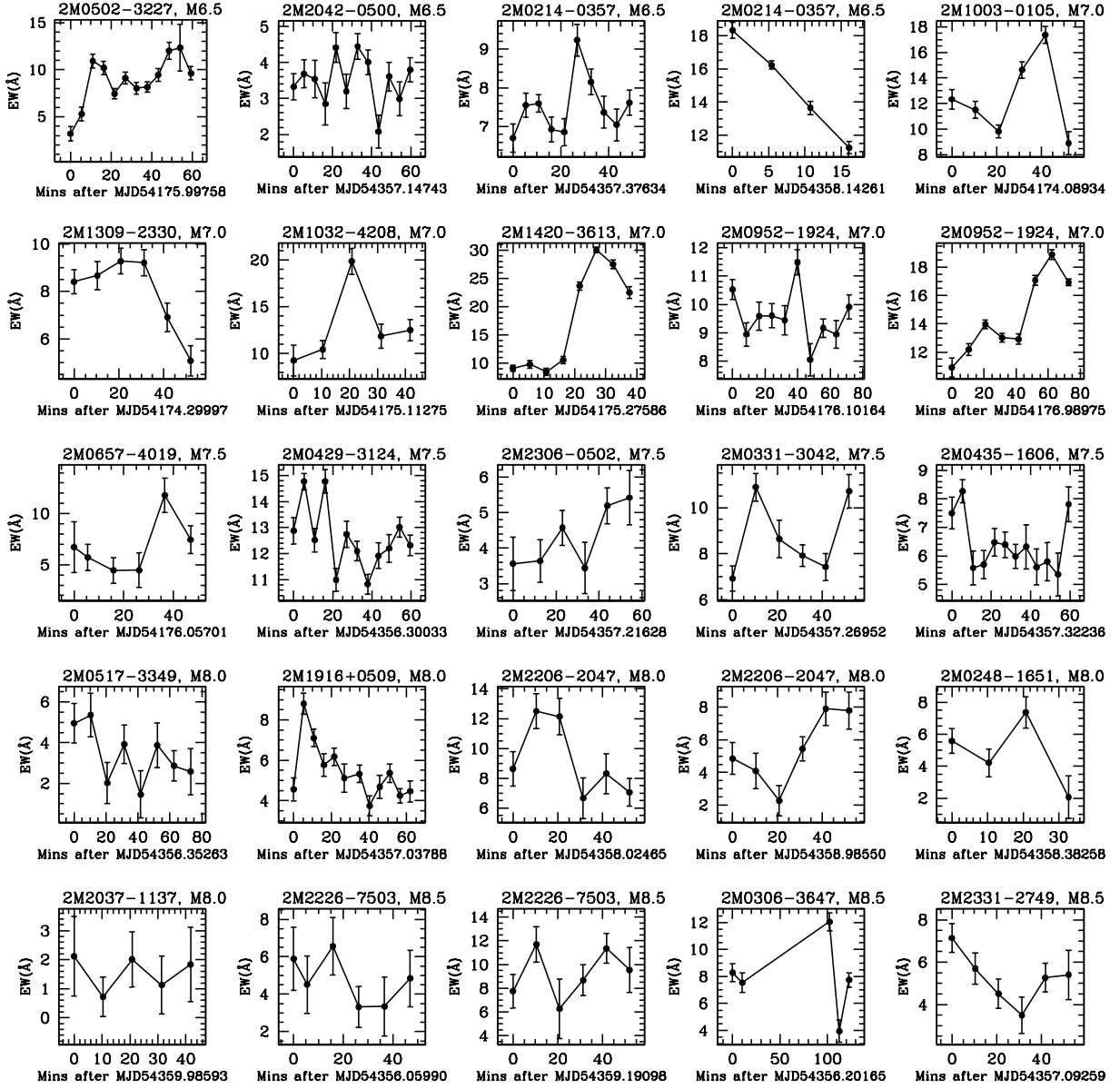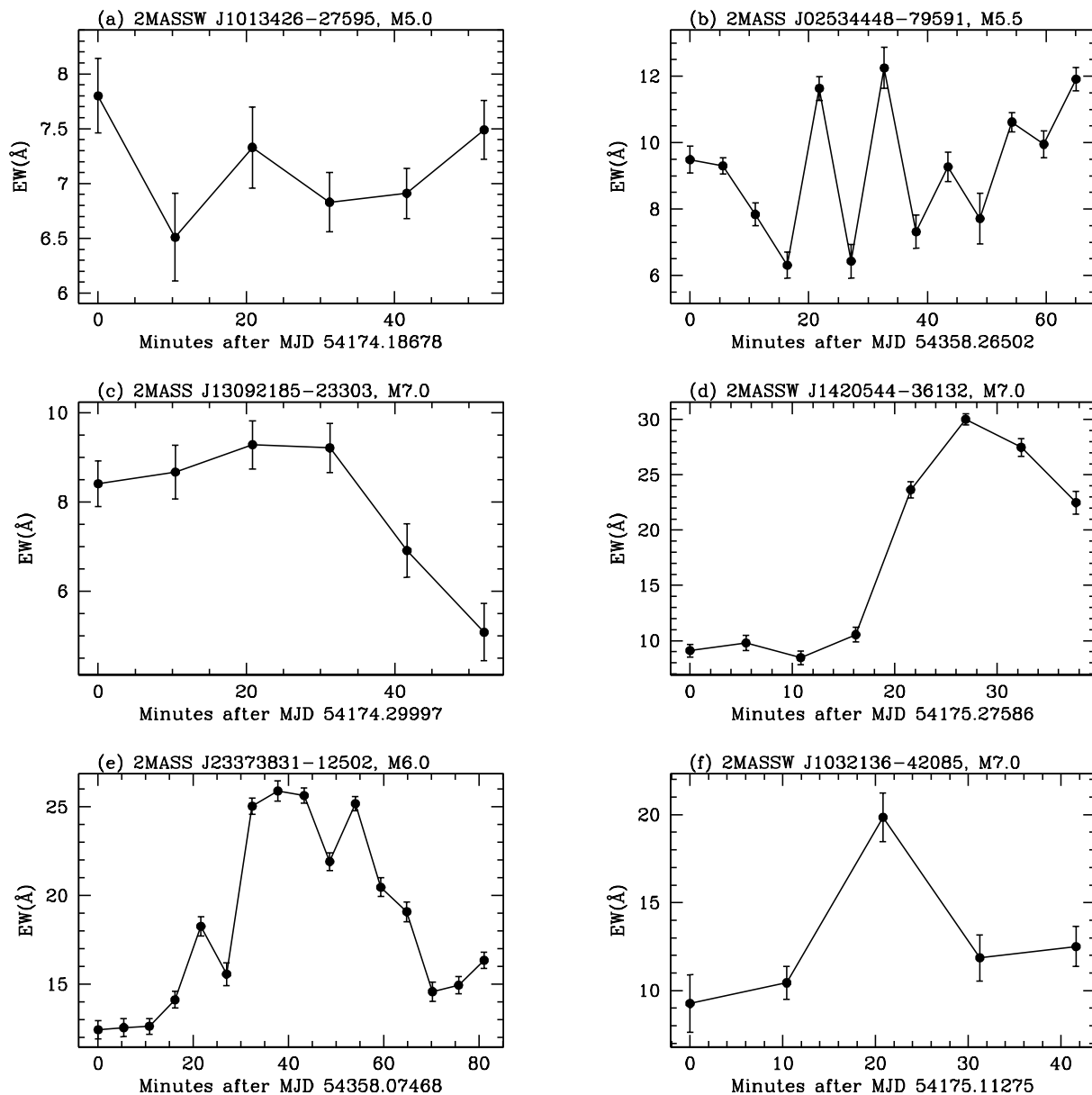
Fig. 2.— Same as Figure 1.

Fig. 3.— Subset of Figures 1 and 2 enlarged for discussion. Figure 3a is an example of a light curve consistent with non-varying EW (see §3). Figures 3b and 3c display examples of objects with rapid and gradual variability, respectively. The other plots show 3 of the objects that displayed the greatest variability during our observations.
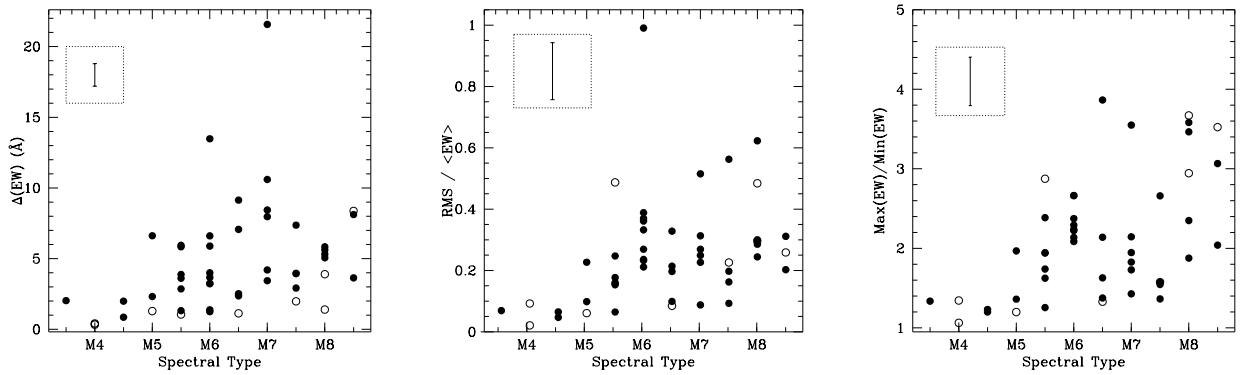
Fig. 4.— Left: Difference between the maximum and minimum Hα EW, Δ(EW), plotted against spectral type. Center: Normalized RMS of the Hα EW light curves of individual observations, plotted against spectral type. Right: Ratio of maximum and minimum Hα EW, R(EW), plotted against spectral type. In all three plots the error bar on the upper left show the median errors. Open circles designate objects identified as non-varying using our χ^2 criterion (§3).
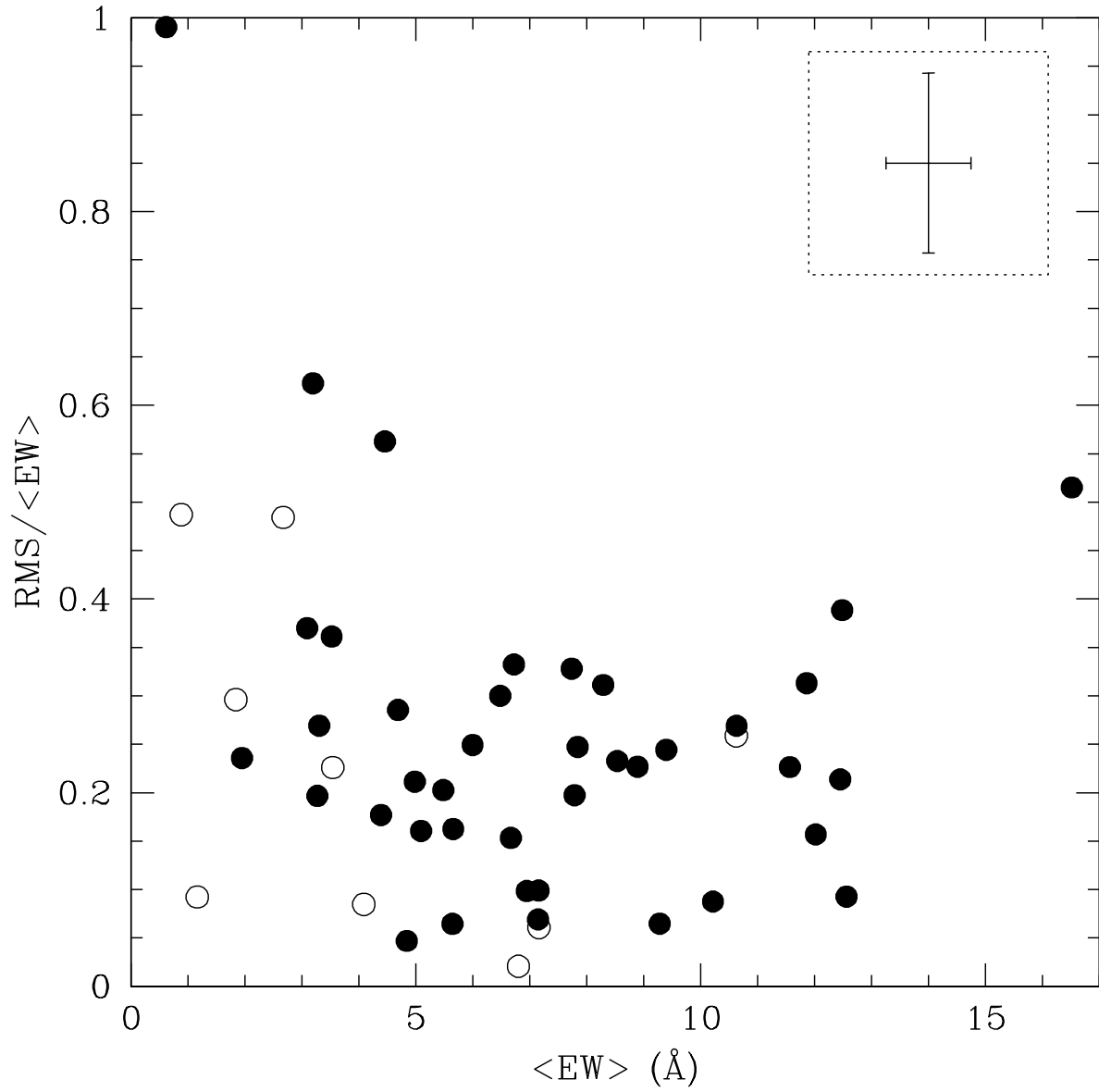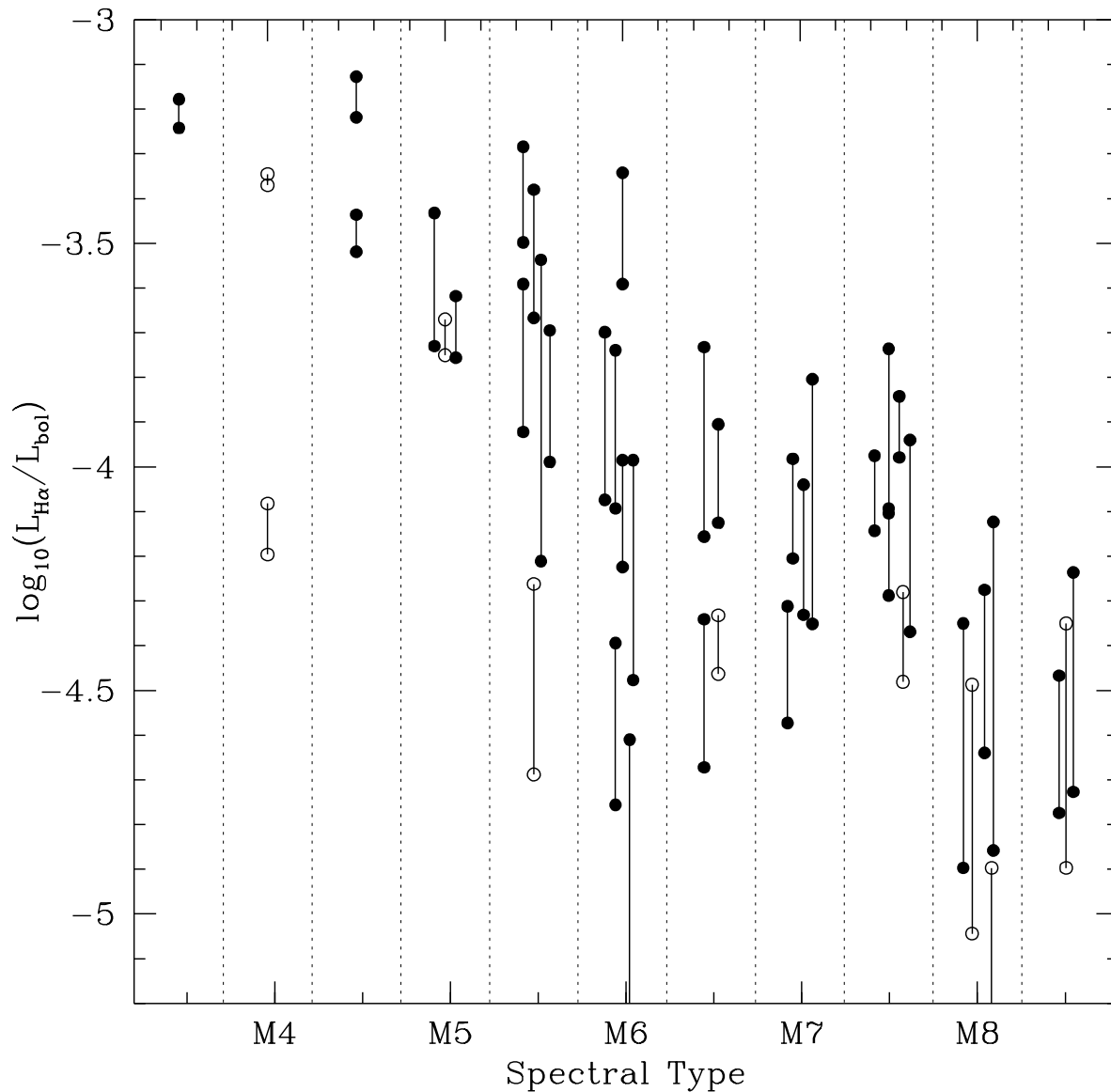
Fig. 5.— Median-normalized RMS of the EW light curves plotted against the median EW. The error bars at upper left show the median errors. Open circles denote objects identified as non-varying through our χ^2 criterion.

Fig. 6.— Logarithmic ratios of $L_{H\alpha}$ and L_{bol}, plotted against spectral type. The solid lines connect the maximum and minimum $L_{H\alpha}/L_{bol}$ values measured for each object. Open circles designate objects identified as non-varying through our χ^2 criterion. The positions of objects are displaced horizontally for clarity, and the dashed vertical lines delineate the spectral types.
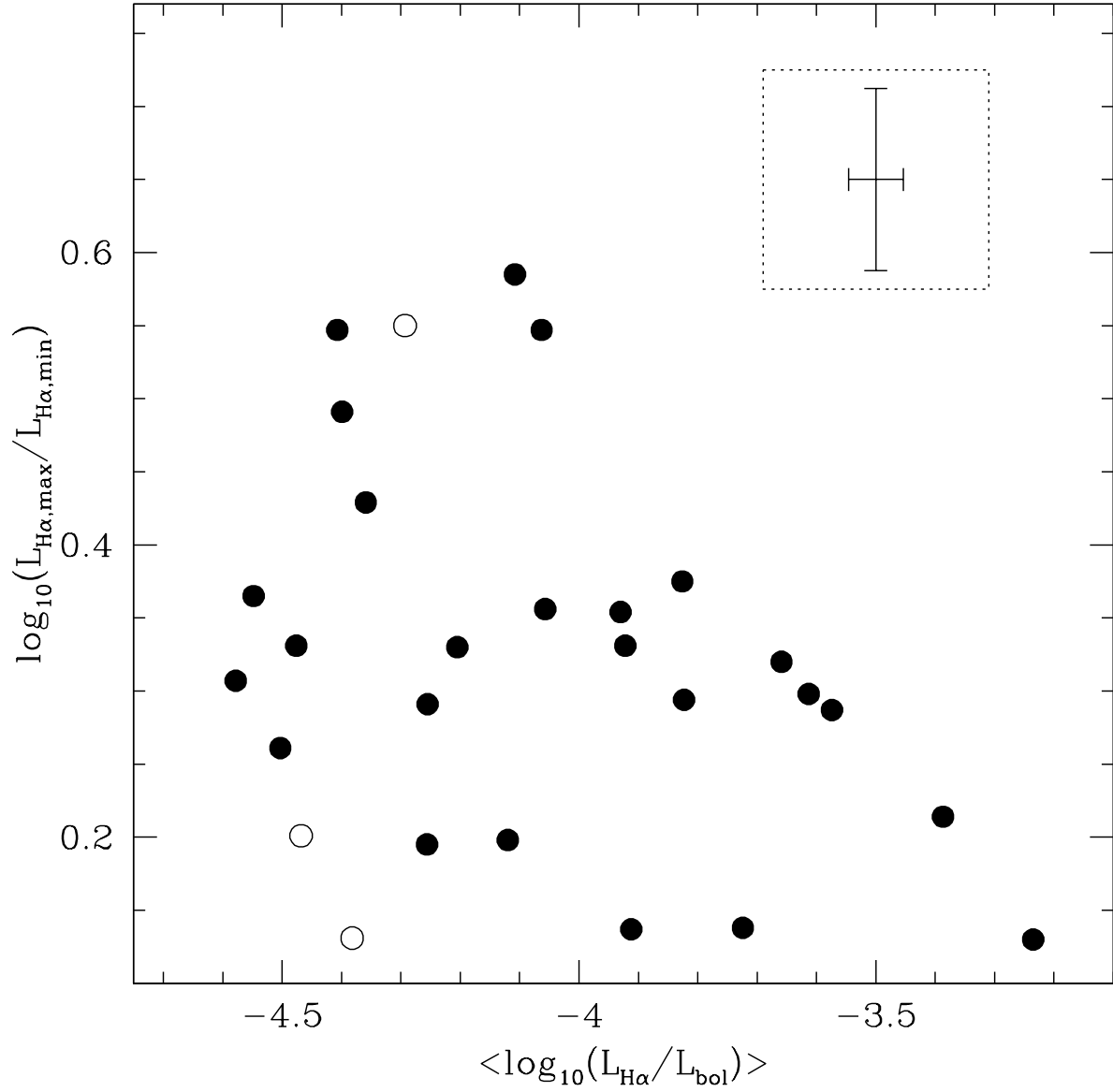
Fig. 7.— Ratio of maximum and minimum Hα luminosity plotted against median Hα luminosity. The error bar on the upper right show the median uncertainty. Open circles denote objects identified as non-varying through our χ^2 criterion.
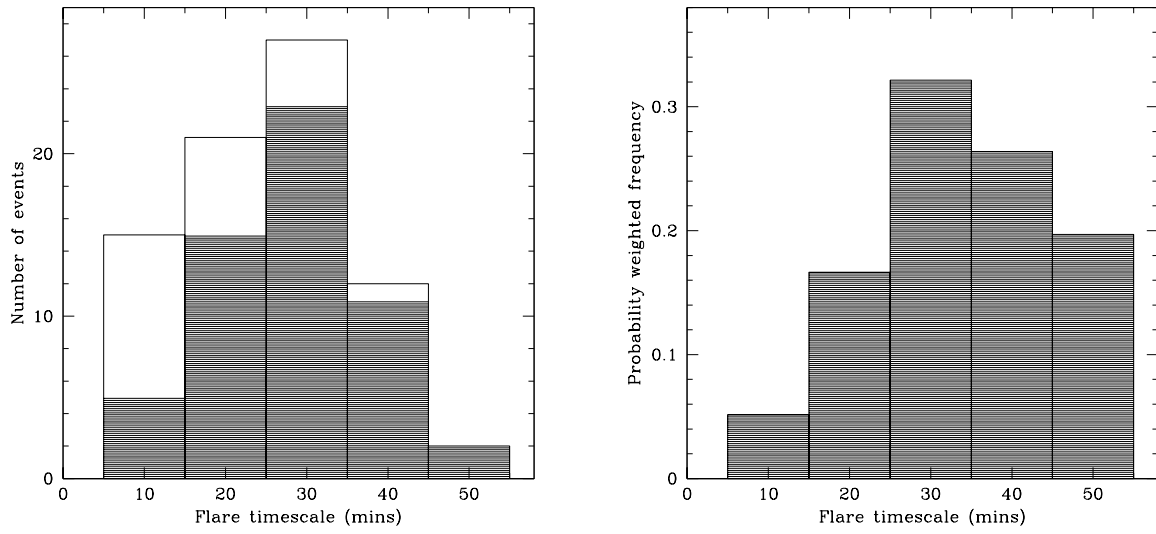
Fig. 8.— Left: Histogram of variability events binned by timescale. Unshaded regions denote partially observed events. Right: Frequency of variability events weighted by the probability of being observed within a finite observing time of about 1 hr, and with the partial events uniformly distributed on timescales equal to or longer than their observed timescale. The normalization is chosen such that the total area is unity.
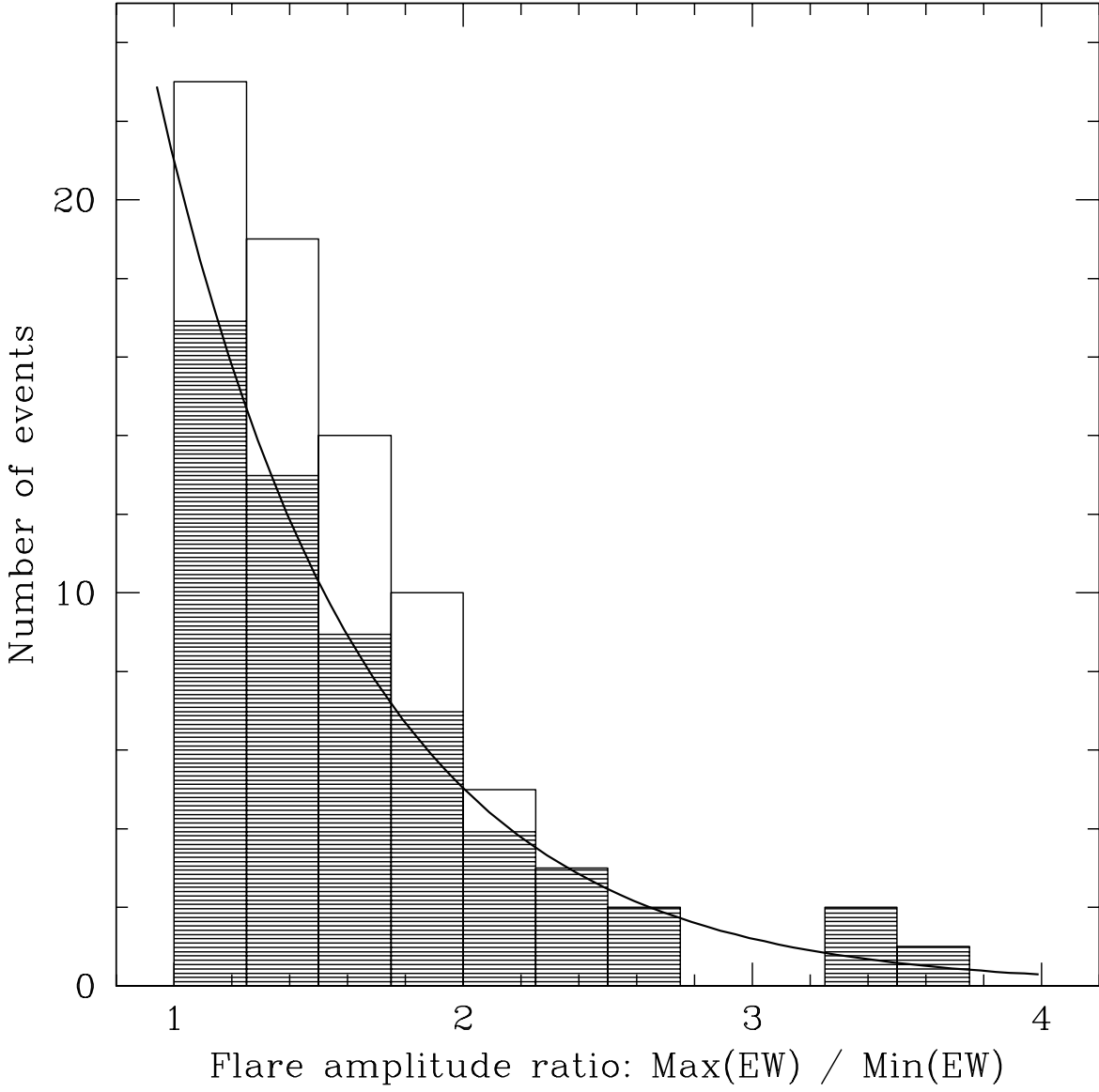
Fig. 9.— Histogram of variability events binned by flare amplitude ratio. The solid curve is an exponential distribution with a decay constant of 0.7. Unshaded regions denote partially observed events.
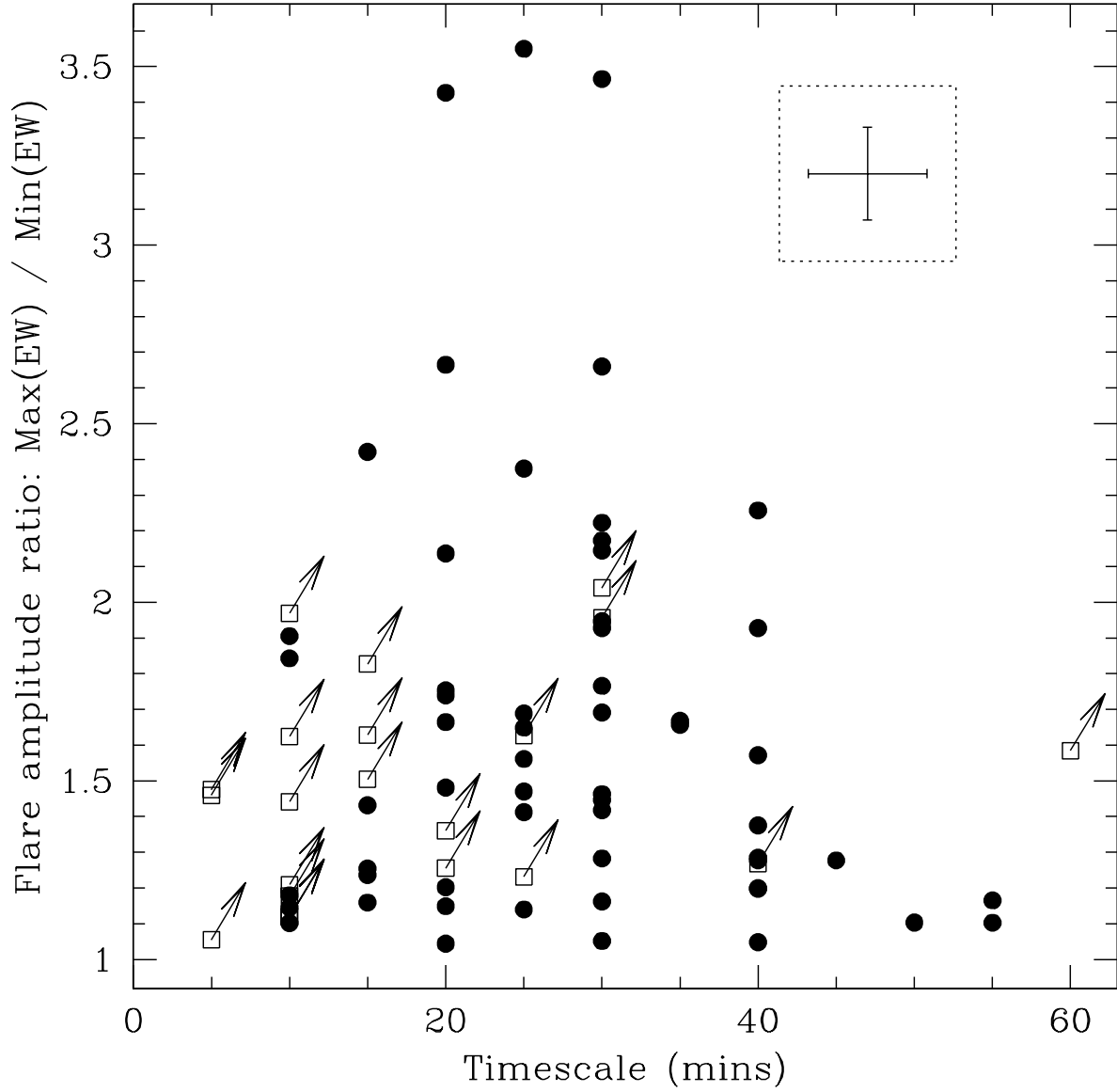
Fig. 10.— Amplitude ratio of variability events plotted against timescale. Square boxes with diagonal arrows denote partially observed events, which are lower limits in both amplitude and timescale. The error bars at the upper right show the median errors.